PAPER

Heterojunction double dumb-bell Ag$_2$Te–Te–Ag$_2$Te nanowires†

Anirban Som and T. Pradeep*

Growth of isolated axial heterojunction nanowires by a solution phase growth process is reported. The dumb-bell shaped nanowires contain two silver telluride sections at the extremes joined by a tellurium section. Reaction of silver nitrate with tellurium NWs in aqueous solution at a molar ratio of 1 : 1 leads to the formation of amorphous partially silver reacted Te NWs. Low temperature (75 °C) solution phase annealing of these silver deficient NWs results in phase segregation producing crystalline Ag$_2$Te and Te phases with clear phase boundaries along the wire axis. Structural characterization of these dumb-bell shaped NWs was performed with different microscopic and spectroscopic tools. Solution phase silver concentration over the course of annealing indicated leaching of silver into the solution during the formation of biphasic NWs. Similar Ag : Te ratios were observed in both partially silver reacted Te NWs and phase segregated Ag$_2$Te–Te–Ag$_2$Te NWs and this was attributed to redeposition of leached silver on the amorphous NW tips which eventually resulted in complete phase segregation. Successful integration of different chemical components in single NWs is expected to open up new application possibilities as physical and chemical properties of the heterostructure can be exploited.

Introduction

Integration of two or more chemically distinct phases into a single nanostructure to make hybrid materials has been a focal point of nanoscale research in recent years as such structures offer new or improved properties in comparison to a mixture of single component systems.[1,2] These properties open up new avenues for the application of hybrid nanomaterials in various fields such as thermoelectrics,[3–6] photocatalysis,[7–10] battery applications,[11] sensors,[12] data storage,[13] etc. Interest in one dimensional (1D) nanostructures has grown considerably over the years as they act as better model systems for studying nanoscale structure–property correlations and effects of quantum confinement.[14,15] Semiconductor nanowires (NWs) offer exciting size dependent optical and electronic properties which make them suitable as the building blocks for semiconductor devices.[16] Tellurium, a narrow band semiconductor

with a band gap of 0.3 eV, has a very strong tendency towards anisotropic growth. In its crystal structure, Te atoms are believed to be bound together through Van der Waals interactions in a hexagonal lattice which leads to preferential formation of 1D structures.[17] This unique property has been exploited by several groups to synthesize several 1D nanostructures like rods,[18,19] wires,[17,20–22] tubes,[23–26] etc. These 1D Te nanostructures have further been utilised as a template for synthesizing different metal telluride nanostructures.[27–33] While several of these single phase NWs have been synthesized, recent efforts have been directed towards the facile synthesis of heterostuctured NWs though reports have been very few.[34] These 1D hetero-nanostructures belong to multiple types. In core–shell structures, the multiple phases are uniform all through the nanowire axis. Zhang *et al.* synthesized Te–Bi and Te–Bi$_2$Te$_3$ core–shell NWs through precursor mediated solution phase reactions.[6] In the category of multiple heterostructure NWs, two phases co-exist in segments in a given NW. Formation of Te–Bi$_2$Te$_3$[35] and Te–CdTe[36] segmented NWs were observed by solid state annealing of supersaturated Bi$_{0.26}$Te$_{0.74}$ and Cd$_{0.28}$Te$_{0.72}$ alloy NWs, respectively. This suggests that non-stoichiometry induces phase separation in NWs. A one pot solution phase synthesis of Bi$_2$Te$_3$–Te nanoplate–nanorod[37] heteronanostructures grown on tips of Te nanorods was reported recently by Wang *et al.*, possibly the only report of an axial heterojunction tellurium-metal telluride nanostructure, although such 'nanobarbells' don't represent a 1D structure. An initial report from our group was on Ag$_5$Te$_3$–HgTe–Ag$_5$Te$_3$ nanowires formed through partial cation exchange,[38] a method earlier reported by Robinson *et al.*[39] Development of novel methods, especially in the solution phase

DST Unit of Nanoscience (DST UNS), Department of Chemistry, Indian Institute of Technology Madras, Chennai 600 036, India. E-mail: pradeep@iitm.ac.in; Fax: +91-44-2257-0545/0509; Tel: +91-44-2257-4208

† Electronic supplementary information (ESI) available: size distribution of Te and Ag$_2$Te NWs, HRTEM and XRD of Te and Ag$_2$Te NWs, EDS of Ag$_2$Te NWs, TEM image and EDS spectra of partially silver reacted Te and the dumbbell shaped NWs, HRTEM, PXRD and solid state annealing data of partially silver reacted Te NWs, variation of diameter along the length of dumb-bell shaped NW, HRTEM images of heterojunction, TEM images and EDS spectra showing the time dependent growth of biphasic NWs, TEM images showing bending and breaking of biphasic system on further annealing, temperature dependence of the growth of biphasic NWs and tuning the length of Te and Ag$_2$Te sections in biphasic NWs. See DOI: 10.1039/c2nr30730h

is important as this enables faster scale-up and development of applications.

Silver telluride, a narrow band semiconductor at room temperature, has attracted considerable interest in recent times due to its various interesting properties. Ag_2Te exhibits a phase change from its low temperature monoclinic phase (β-Ag_2Te) to its high temperature fcc phase (α-Ag_2Te) at $\sim$423 K, where it is a superionic conductor.[40] It is also known to show large magnetoresistance[41,42] and magnetothermopower.[43] Ag_2Te exhibits high electron mobility and low thermal conductivity, and is desirable for its high figure of merit (ZT) for thermoelectric applications.[44] These properties become richer when studied at the nanoscale due to the confinement of electronic states and a maximum Seebeck coefficient of -170 μV K^{-1} was observed in NWs.[45]

In the present work, an extremely efficient method to form isolated and dispersable axial heterojunction Ag_2Te–Te–Ag_2Te NWs is reported. The morphology of these heterojunction NWs resembles that of dumbbells due the larger diameter of the Ag_2Te sections compared to Te. Till now dumbbell like hybrid nanostructures have been achieved either by selective growth of the second component on the tips of nanorods[37,46–48] or by preferential etching of core–shell nanorods.[49] These techniques require special seeds, surfactants and experimental conditions. Our synthetic procedure is a combination of the reaction between silver and tellurium NWs and subsequent annealing of those partially silver reacted NWs as shown in the schematic. Both the steps were carried out in the aqueous phase (see the experimental section). By carefully adjusting the annealing conditions, rod shaped Ag_2Te sections were grown at both ends of Te NWs. To the best of our knowledge, this is first time report of rod shaped secondary structures grown along the wire axis to produce dumbbell shaped heterostructures of tellurium in solution.

Experimental section

Sodium dodecyl sulfate (SDS, $C_{12}H_{25}O_4SNa$, 99%) was obtained from RANKEM, India. Tellurium dioxide (TeO_2, 99.9%) powder was purchased from Alfa Aesar. Silver nitrate ($AgNO_3$) and hydrazine monohydrate ($N_2H_4\cdot H_2O$, 99–100%) were purchased, respectively from SD Fine Chemicals and Fisher Scientific, India. All the chemicals were used as obtained without any further purification. Deionized water was used throughout the study.

Preparation of Ag_2Te–Te–Ag_2Te involves three steps as described below:

Te NWs were prepared by the chemical method; originally reported by Chang et al.[17] In a typical procedure, 24 mg of TeO_2 powder was slowly added to a beaker containing 10 mL of hydrazine monohydrate. The reaction was allowed to continue at room temperature under constant magnetic stirring. The powder dissolved completely and the color of the solution changed from colorless to blue indicating the formation of Te NWs. After 1 h, the solution was diluted 10-fold with 10 mM SDS, in order to control the length of the NWs. The as-prepared solution was purified by centrifugation at 8000 rpm for 5 minutes. The residue was redispersed in deionized water. The centrifugation–redispersion cycle was repeated twice to remove the unreacted species and excess surfactant.

Cleaned Te NWs were used as a template for the synthesis of Ag_2Te NWs. In a typical synthetic procedure, 3 mL of 10 mM $AgNO_3$ solution was added to a dispersion of 10 mL Te NWs ($\sim$1.5 mM with respect to tellurium) under constant magnetic stirring. The color of the suspension changed from blue to dark brown within a few minutes indicating the formation of Ag_2Te NWs. Stirring was continued for 6 h and finally clean nanowires were obtained after centrifugation at 6000 rpm for 5 minutes which were redispersed in deionized water. Partially silver reacted Te NWs, used as the starting material for synthesizing the Ag_2Te–Te–Ag_2Te dumbbell shaped nanowires, were prepared following the same protocol as for the Ag_2Te NWs; only change was that the amount of $AgNO_3$ (10 mM) added was 1.5 mL.

Formation of Ag_2Te–Te–Ag_2Te heterojunction nanowires were observed upon annealing these partially silver reacted Te NWs. Annealing was done at 75 °C for 24 h in aqueous solution. Outline of the experiments is shown schematically in Scheme 1. An EYELA organic synthesizer was used to ensure that the same temperature was maintained throughout the study.

Supernatant for ICP-OES measurements was collected from the heated suspension at different time intervals by centrifugation of the suspension at 18 000 rpm for 3 minutes.

Instrumentation

UV-visible extinction spectra for all the samples were recorded on a PerkinElmer Lambda 25 spectrophotometer. High-resolution transmission electron microscopy (HRTEM) was performed on a JEOL 3010 (JEOL Ltd.), 300 kV instrument equipped with a UHR polepiece. Energy dispersive X-ray spectroscopy (EDS) was carried out with an Oxford EDAX housed in the TEM. Samples for TEM analysis were prepared by dropping the dispersion on carbon coated copper grid and drying in ambient condition. X-Ray diffraction (XRD) data were collected with a Bruker AXS, D8 Discover diffractometer using Cu-Kα (λ = 1.54 Å) radiation. All the peaks were assigned and compared with the database published by the Joint Committee on Powder Diffraction Standards (JCPDS). X-Ray photoelectron
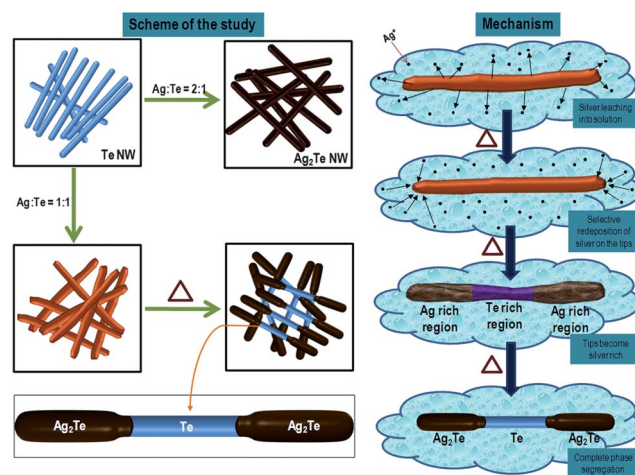
Scheme 1 Schematic representation of the solution phase growth of dumbbell shaped Ag_2Te–Te–Ag_2Te. The proposed mechanism for the formation of biphasic nanowires is also shown.

spectroscopy (XPS) measurements were done using an Omicron ESCA Probe spectrometer with polychromatic Mg Kα X-rays ($h\nu$ = 1253.6 eV). The X-ray power applied was 300 W. The pass energy was 50 eV for survey scans and 20 eV for specific regions. Sample solution was spotted on a molybdenum sample plate and dried in vacuum. The base pressure of the instrument was 5.0×10^{-10} mB. The binding energy was calibrated with respect to the adventitious C 1s feature at 285.0 eV. ICP-OES data for determining silver concentration in the supernatant was collected on a PerkinElmer Optima 5300 DV spectrometer.

Results and discussion

Ag_2Te NWs were made starting from tellurium NWs.[28] The blue color of the dispersion of Te NWs turned dark brown upon their almost instantaneous transformation to Ag_2Te NWs. This is also manifested by the disappearance of two distinct peaks in the UV-visible extinction spectrum of tellurium NWs and simultaneous appearance of a broad band (Fig. 1A). Upon this transformation, a 15% increase in length and 33% increase in the diameter of the NWs (~103% volume increase) was observed which can be seen from the length and diameter distributions of Te and Ag_2Te NWs (Fig. S1†). This is on par with the volume increase reported by Moon et al.[33] The EDS spectrum of Ag_2Te NWs (Fig. S2†) showed a Ag : Te ratio ~2 : 1. The slight bending observed in some of the Ag_2Te NWs is possibly a consequence of large strain, induced by volume change. Both the NWs were found to be crystalline from HRTEM and powder XRD (PXRD) analyses (Fig. S2†). No Te^{4+} phases were observed in the PXRD pattern indicating no disproportionation of Te into Te^{4+} and Te^{2-}. No significant structural changes were observed upon heating the Ag_2Te NWs in solution up to 24 hours.

However, addition of lesser amount of Ag^+ so as to produce an Ag : Te ratio of ~1 : 1 causes significant changes in the morphology (Fig. 1D). The UV-visible extinction spectrum of these partially silver reacted NWs (trace c, Fig. 1A) shows two distinct features, one broad band around 570 nm which is red shifted compared to the one for Ag_2Te at 470 nm, but blue shifted compared to peak II of Te NWs (at 796 nm) and another at 288 nm which is slightly blue shifted compared to peak I of Te NWs (at 293 nm). Incorporation of silver in the NWs was confirmed from the EDS spectrum (Fig. S3†) and it shows a Ag : Te atomic ratio of 1 : 0.96 in the formed NWs. Presence of any crystalline phase is not indicated in both HRTEM and PXRD (Fig. S4†). Although the AgTe phase is reported in the literature, it does not form under normal atmospheric conditions and is known to be metastable.[50]

Solution phase annealing of these silver deficient NWs at 75 °C for 24 hours leads to the formation of dumbell shaped NWs (Fig. 1E) predominantly. A definite contrast difference between the end segments and the middle one is observable in the TEM image of a single NW (Fig. 1F) and it hints towards the presence of two different components in those sections. The UV-visible extinction spectrum of these NWs (trace d, Fig. 1A) shows three dominant features. The peaks at 290 and 682 nm can be correlated with peak I and peak II of Te NWs of shorter length and the other appears as a band in-between these two peaks with a maximum around 370 nm. Presence of three bands in the UV-visible spectrum indicated towards the successful integration
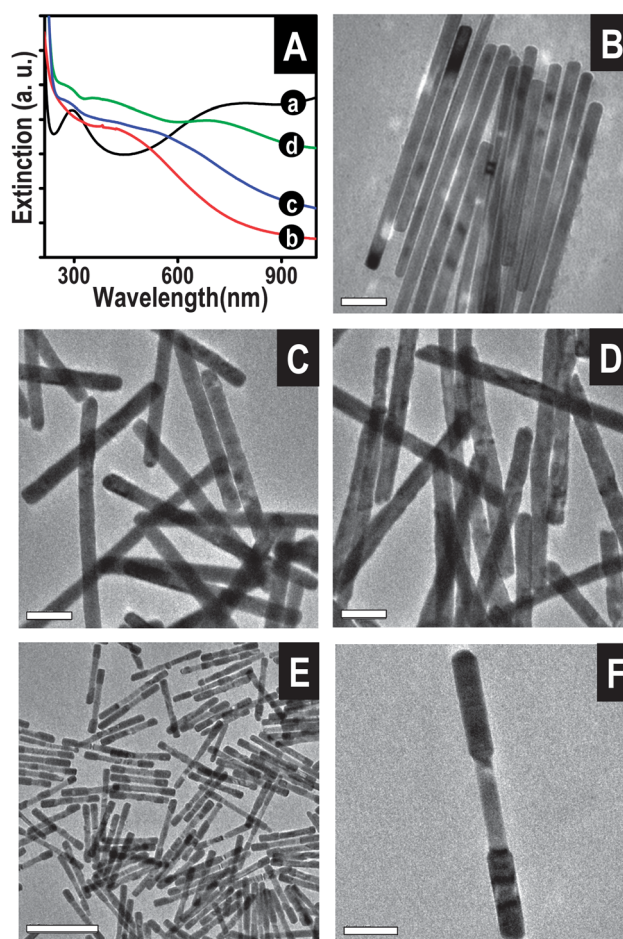
Fig. 1 (A) UV-vis extinction spectra of partially silver reacted Te nanowire dispersion before (trace c) and after (trace d) 24 h annealing at 75 °C. Spectra of Te and Ag_2Te nanowires (traces a and b, respectively) are shown for comparison. (B) TEM image of Te nanowires showing their straight morphology. (C) TEM image of Ag_2Te nanowires which are slightly bent compared to the parent Te nanowires. The increase in diameter is evident. (D) Large area TEM image of partially silver reacted tellurium nanowires, changes in nanowire morphology from Te nanowire are observable. (E) Large area TEM image of the nanowires formed after solution phase annealing. (F) TEM image of a single nanowire formed upon annealing; its morphology resembles that of a dumbbell. The scale bar in E is 500 nm and is 100 nm in the other images.

of Te and Ag–Te phases within the same nanowire. The average diameter of the middle and two end sections of the NWs (Fig. S5†) also indicated the presence of Te and Ag–Te phases in those sections of the NWs. Average diameter of the middle section was 32 nm (same as the average diameter of the parent Te NWs) and that of the end sections was 44 nm (very much comparable with the average diameter of Ag_2Te and partially silver reacted Te NWs).

EDS and HRTEM analyses of the NWs clearly reveal their biphasic nature. EDS intensity maps of Te and Ag (Fig. 2C and D, respectively) show the presence of Te throughout the length of the NW whereas Ag is limited within two end segments of the NW. Moreover, the EDS spectrum collected from area 2 (Fig. 2F) in Fig. 2A indicated the presence of only Te whereas that from area 1 (Fig. 2E) indicated it to be a compound with an atomic ratio of 66% Ag and 34% Te, which is close to the
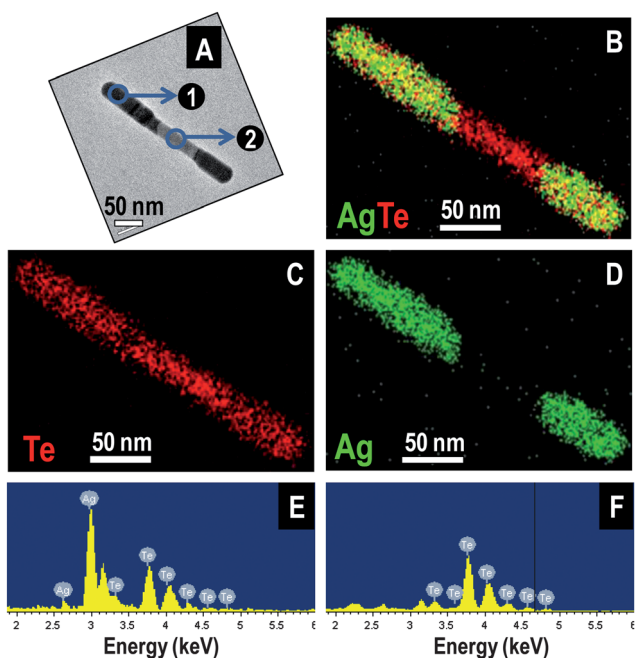
Fig. 2 EDS analysis to prove the biphasic nature of the dumbbell shaped nanowires. (A) TEM image of the dumbbell shaped nanowire chosen for EDS analysis. (B) Combined intensity maps for Ag and Te for the nanowire. (C) Te Lα intensity map across the length of the dumbbell shaped nanowire. Note that the intensity in the middle region is higher than from the tips. (D) Ag Lα intensity map showing that silver is limited only to both the ends. (E) EDS spectrum collected from area 1 in A showing the presence of both Ag and Te in the atomic ratio of 2 : 1. (F) EDS spectrum from area 2 in A, showing the presence of only Te in the middle section.

stoichiometry of Ag_2Te, the low temperature equilibrium phase in the Ag–Te phase diagram.[50]

Lattice mismatch between two components in heterostructures generally leads to a large number of crystal defects in them. Nanowire geometry is known to facilitate the formation of defect free crystal structures required for the fabrication of high efficiency devices, as the strain induced due to lattice mismatch is relaxed at the NW side walls.[51] A HRTEM image of one of the modified NWs shows the presence of perfectly crystalline Te and Ag_2Te regions (Fig. 3A) which are shown separately in the insets. Inset in Fig. 3B shows a low resolution image of a biphasic nanowire and a high resolution image from the marked area clearly indicates the presence of a definite interface across Te and Ag_2Te phases in the biphasic NWs. Detailed HRTEM analysis of the heterojunction for the same area covering the entire diameter of NW is shown in Fig. S6†.

Presence of crystalline Te and β-Ag_2Te phases in the same nanostructure was also confirmed from the PXRD pattern of the NWs, shown in Fig. 4A. All the peaks can be indexed to either the hexagonal phase of Te or monoclinic phase of Ag_2Te. The transformation of Te NW to Ag_2Te NW is known to be top-otactic where (100) directed hexagonal Te phase converts into (110) directed monoclinic Ag_2Te phase.[33] This results in the large increase in the lateral dimension of Ag_2Te phase. Strain along the c-axis of Te NW is minimized in this process which in turn helps in the formation of defect free biphasic NW system. The JCPDS patterns of Te (JCPDS: 36-1452) and Ag_2Te (JCPDS: 34-0142) are shown in the inset and they match with the data. XPS spectra in the Te 3d region for the biphasic NWs along with those of Te and Ag_2Te NWs are shown in Fig. 4B. The spectra indicate that the tellurium phase does not oxidise to Te^{4+} during the annealing
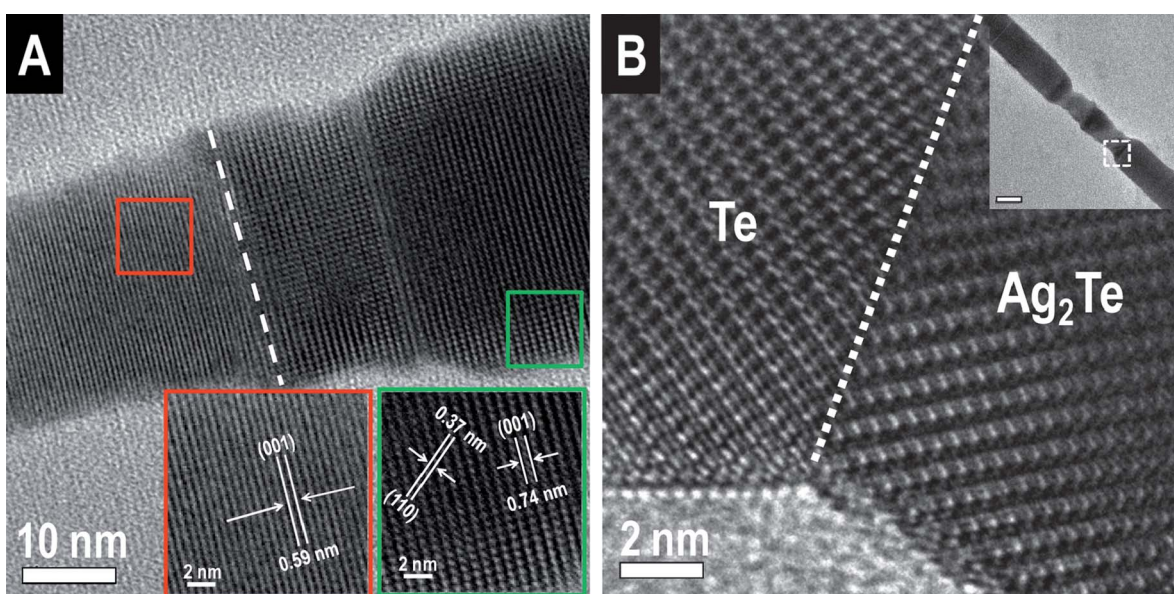
Fig. 3 HRTEM analysis of the biphasic nanowires. (A) Lattice resolved TEM image of a dumbbell shaped nanowires showing the presence of both hexagonal Te and monoclinic Ag_2Te phases (areas marked by red and green boxes, respectively) in the same nanowire. Corresponding lattice planes are marked in expanded views of those areas, shown in the insets. (B) HRTEM image showing the presence of a well defined phase boundary in the nanowire. Inset of the image shows a low magnification image of the nanowire. Area corresponding to the high resolution image is marked. Scale bar for the inset image is 100 nm.
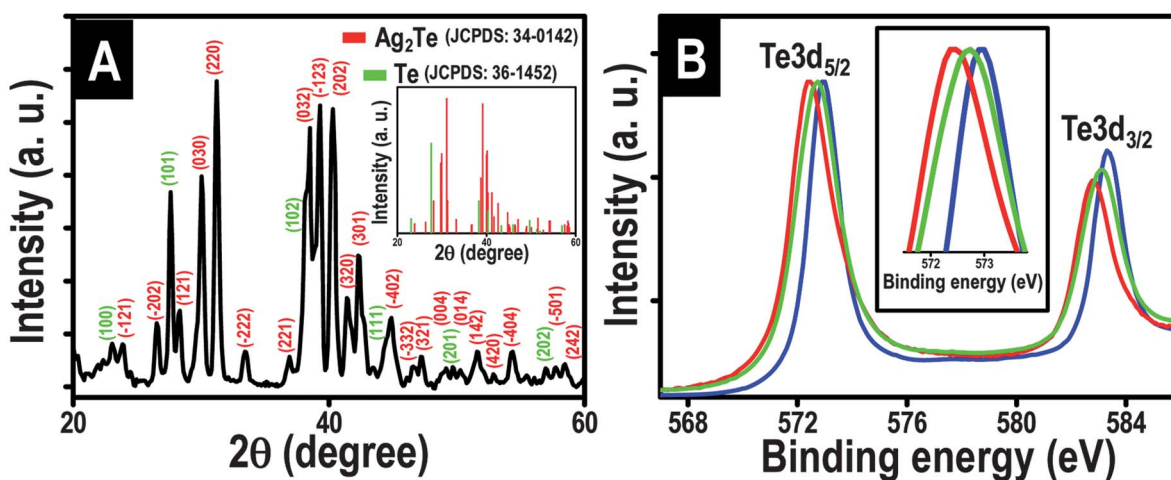
Fig. 4 (A) XRD pattern of the biphasic nanowires. All the peaks have been assigned to Te (indexed in green) and β-Ag$_2$Te (indexed in red). JCPDS file number and corresponding pattern for Te and Ag$_2$Te phases are given in the inset. (B) XPS spectra of Te 3d region of the biphasic NWs (green trace) in comparison with Te and Ag$_2$Te NWs (blue and red traces, respectively). No Te (IV) phases were observed. Inset in B shows a zoomed in view of Te 3d$_{5/2}$ region for the three NWs.
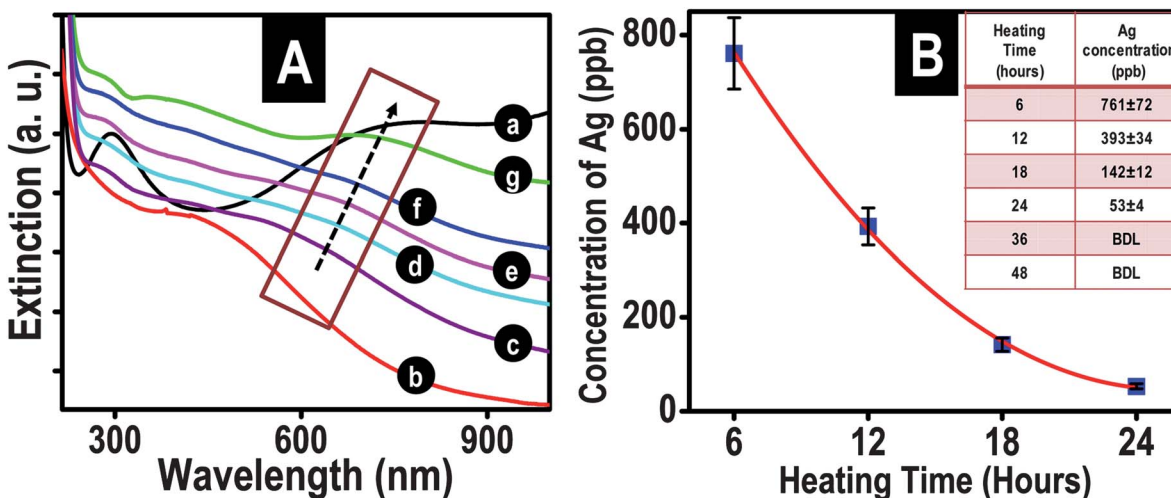
Fig. 5 Growth of biphasic nanowires with annealing time monitored with UV-visible spectroscopy. Traces d–g represent UV-visible spectra of the nanowires after 6, 12, 18 and 24 hours of annealing. Spectra for Te, Ag$_2$Te and partially Ag reacted Te NWs (traces a, b and c, respectively) are given for comparison. Emergence of peaks to Te NWs is evident with annealing. (B) Solution state measurement showing the decreasing concentration of silver with annealing time. Inset of the figure shows the concentrations. BDL means below detection limit.

process which correlate with the XRD data. This is another advantage of this solution state annealing process as Te can oxidise during solid state annealing in the presence of air. Residual hydrazine present creates a reducing environment in the solution and inhibits the oxidation process. Te 3d$_{5/2}$ binding energies of Te and Ag$_2$Te NWs appear at 573.1 and 572.5 eV and it is at 572.8 eV for the biphasic NWs. The peaks for biphasic NWs appear significantly broad which most likely is due to the presence of both Te(0) and Te^{2-} phases. This corroborates with the other observations.

Formation of these biphasic NWs with increasing heating time was monitored with UV-vis spectroscopy and transmission electron microscopy. Fig. 5A represents a change in the extinction spectrum of NWs with heating time which has been compared with the spectrum of the parent Te (trace a) and Ag$_2$Te

(trace b) NWs. A gradual red shift (shown by an arrow) in the band maxima of partially silver reacted NWs with annealing time was seen; attributed to growth and increase in length of the Te region in the NW body.[17] The observation predicted from the UV-vis data was confirmed from the TEM images taken by stopping the reaction at different time intervals during solution phase annealing (Fig. S7†).

Kinetic control of crystallization is often known to produce an amorphous phase initially which can be non-stoichiometric and is prone to phase transformations.[52] This corroborates with the amorphous nature of the partially silver reacted Te NWs. Phase segregation and crystallization observed in these NWs upon annealing possibly originates from the fact that only phase transformation in the NWs would lead to the formation of a metastable AgTe phase. For a better understanding of the

mechanism of formation of the biphasic crystalline NWs from amorphous partially silver reacted NWs, solution phase concentration of silver was measured with annealing time (Fig. 5B). The data show a high concentration of silver in the dispersion. The silver detected in the solution is bound to originate from the silver reacted Te NWs upon annealing as no unreacted silver in the solution was detected following the addition of $AgNO_3$ into Te NWs. This suggests an important role for the solubility product of the system in the transformation. High solubility of partially silver reacted Te nanowires indicates that the transformation occurs directly from the amorphous phase and does not include transformation into metastable crystalline AgTe phase. The solubility product of a nanoscale solid is given by the following equation:[33]

$$\log K_{sp}^* = \log K_{sp,bulk} + 2\gamma A_m / [3\log(RT)] \qquad (1)$$

where K_{sp}, γ and A_m are the solubility product, surface tension and the molar surface area of the solute, respectively. As for a nanoscale solid, molar surface area increases several fold compared to its bulk counterpart; the solubility product and hence solubility increases. The amorphous phase of a solute can often be highly soluble over its crystalline counterpart. For instance, amorphous calcium carbonate (ACC) is highly soluble compared to its crystalline counterparts like calcite, vaterite, etc.[52] Temperature is a basic parameter to manipulate the solubility of ionic solids and in most of the cases, solubility increases with temperature. In the case of partially Ag reacted Te NWs, silver comes out into solution at a higher solution temperature and redeposits onto the NWs. We did not observe the presence of any Te species in the supernatant which makes us conclude that only silver leaches from the NWs into the solution during the annealing process. Redeposition of silver happens preferentially on the NW tips which is most likely a result of higher reactivity of the tips than the body as may be proposed from the gold growth on Te NWs.[53] This is also well-known for 1D anisotropic systems like gold nanorods. It is due to the higher energy surfaces at the tips or due to poor surfactant stabilization there. In a few of the biphasic NWs, the Ag_2Te section does not form exactly at the end which possibly results from the presence of high energy defect sites on the side faces of NWs which act as re-deposition sites for silver. TEM images taken at different annealing times (Fig. S7†) indicate smoothing of the tips of the NWs upon annealing compared to the irregular nature of the tips of partially silver reacted Te NWs (Fig. 1D) and this possibly results from the deposition of silver on the tips. EDS spectra taken from the middle and end sections of the NWs after different annealing times (Fig. S8†) also support this formation mechanism. The process of silver coming out into solution and redeposition goes on at high solution temperature and results in gradual enrichment of silver content around the tips of the NWs whereas middle sections become depleted in silver. The formation process is shown in Scheme 1. This process stops once complete phase segregation is achieved and Ag_2Te–Te–Ag_2Te NWs are formed which show a very similar Ag : Te ratio to the Ag reacted Te NWs and dumbbell shaped Ag_2Te–Te–Ag_2Te NWs (Fig. S3†).

Formation of Ag_2Te may well be the driving force for the phase segregation observed. Enthalpy of mixing reaches a minimum for a ratio of 2 : 1 of silver and tellurium across the whole range of atomic percentages[50] and this possibly facilitates the formation of the Ag_2Te phase. The basic nature (pH ~14) of the dispersion arising out of the presence of excess hydrazine used in the Te NW preparation may also lead to exclusive formation of Ag_2Te as the Ag–Te phase.[13,54] On the other hand, because of the high thermodynamic stability of the monoclinic β-phase at low temperatures, it has a low solubility product and so once the Ag_2Te phase is formed, the reaction stops. Remember that no morphological changes were observed upon annealing of Ag_2Te NWs under the same conditions.

Formation of heterojunction NWs from partially silver reacted NWs by annealing was found to be solely a solution state process as solid state annealing at the same temperature was ineffective to bring out changes in the nanowire morphology (Fig. S4†). On further annealing beyond 24 hours in solution, initially bending and then breaking of the NWs was observed (Fig. S9†). The effect of annealing temperature on the growth of biphasic NWs was also probed through both UV-visible spectroscopy and TEM (Fig. S10†). When the annealing temperature was maintained at 50 °C, a change in the morphology of tips was observed but no distinct phase separation was obtained. Upon keeping the annealing temperature at 70 °C, the NWs produced had a dumbbell shape but complete phase segregation was not observed in HRTEM after 24 hours. Annealing at a higher temperature (90 °C) leads to the formation of aggregated products. These aggregates contain some silver telluride particles along with some bent wire-like structures. Though wire-like structures were rich in tellurium, presence of silver in them proves that the structures break down before complete phase segregation is achieved (Fig. S10†). This possibly is a result of higher thermal energy put into the system which makes the system more prone towards bending and breaking.

Conclusions

In summary, we have demonstrated a new methodology for the fabrication of axial heterojunction nanowires in which two ends of the Ag_2Te segments are connected through a Te section through low temperature solution phase annealing. Silver comes out into the solution at 75 °C and re-deposits on the tips of partially silver reacted Te NWs. This leads to the formation of a stable monoclinic Ag_2Te phase around the tips while the middle section gradually becomes Te rich and finally the hexagonal Te phase is formed. The morphology of resulting NWs resembles dumbbells which were characterized by UV-vis spectroscopy, TEM, EDS, PXRD and XPS. The presence of the semiconducting Te phase between Ag_2Te regions in the biphasic NWs would reduce the lattice thermal conductivity by blocking scattering of phonons along the wire axis and this could result in the enhancement of the thermoelectric efficiency over Ag_2Te NWs. Tuning the length of Ag_2Te sections is also possible by controlling the amount of $AgNO_3$ added (Fig. S11†). It may also be possible to prepare other heterojunction nanostructures following this route. We are pursuing research in these directions.

Acknowledgements

References

1 R. Costi, A. E. Saunders and U. Banin, *Angew. Chem., Int. Ed.*, 2010, **49**, 4878–4897.
2 G. Zhu and Z. Xu, *J. Am. Chem. Soc.*, 2011, **133**, 148–157.
3 Y. Zhang, H. Wang, S. Kräemer, Y. Shi, F. Zhang, M. Snedaker, K. Ding, M. Moskovits, G. J. Snyder and G. D. Stucky, *ACS Nano*, 2011, **5**, 3158–3165.
4 R. J. Mehta, C. Karthik, B. Singh, R. Teki, T. Borca-Tasciuc and G. Ramanath, *ACS Nano*, 2010, **4**, 5055–5060.
5 A. Purkayastha, Q. Yan, M. S. Raghuveer, D. D. Gandhi, H. Li, Z. W. Liu, R. V. Ramanujan, T. Borca-Tasciuc and G. Ramanath, *Adv. Mater.*, 2008, **20**, 2679–2683.
6 G. Zhang, W. Wang and X. Li, *Adv. Mater.*, 2008, **20**, 3654–3656.
7 L. Amirav and A. P. Alivisatos, *J. Phys. Chem. Lett.*, 2010, **1**, 1051–1054.
8 C. Harris and P. V. Kamat, *ACS Nano*, 2010, **4**, 7321–7330.
9 Y. Shemesh, J. E. Macdonald, G. Menagen and U. Banin, *Angew. Chem., Int. Ed.*, 2011, **50**, 1185–1189.
10 A. Vaneski, A. S. Susha, J. Rodríguez-Fernández, M. Berr, F. Jäckel, J. Feldmann and A. L. Rogach, *Adv. Funct. Mater.*, 2011, **21**, 1547–1556.
11 W. Zhou, C. Cheng, J. Liu, Y. Y. Tay, J. Jiang, X. Jia, J. Zhang, H. Gong, H. H. Hng, T. Yu and H. J. Fan, *Adv. Funct. Mater.*, 2011, **21**, 2439–2445.
12 L. L. Xing, S. A. Yuan, Z. H. Chen, Y. J. Chen and X. Y. Xue, *Nanotechnology*, 2011, **22**, 215501.
13 S. K. Batabyal and J. J. Vittal, *Chem. Mater.*, 2008, **20**, 5845–5850.
14 Y. N. Xia and P. D. Yang, *Adv. Mater.*, 2003, **15**, 351.
15 M. Law, J. Goldberger and P. Yang, *Annu. Rev. Mater. Res.*, 2004, **34**, 83–122.
16 C. M. Lieber and Z. L. Wang, *MRS Bull.*, 2007, **32**, 99–108.
17 Z.-H. Lin, Z. Yang and H.-T. Chang, *Cryst. Growth Des.*, 2008, **8**, 351–357.
18 Z. Liu, Z. Hu, J. Liang, S. Li, Y. Yang, S. Peng and Y. Qian, *Langmuir*, 2004, **20**, 214–218.
19 Z. Liu, Z. Hu, Q. Xie, B. Yang, J. Wu and Y. Qian, *J. Mater. Chem.*, 2003, **13**, 159–162.
20 Y.-J. Zhu, W.-W. Wang, R.-J. Qi and X.-L. Hu, *Angew. Chem., Int. Ed.*, 2004, **43**, 1410–1414.
21 Q. Lu, F. Gao and S. Komarneni, *Langmuir*, 2005, **21**, 6002–6005.
22 Q. Lu, F. Gao and S. Komarneni, *Adv. Mater.*, 2004, **16**, 1629–1632.
23 B. Mayers and Y. Xia, *Adv. Mater.*, 2002, **14**, 279–282.
24 X.-L. Li, G.-H. Cao, C.-M. Feng and Y.-D. Li, *J. Mater. Chem.*, 2004, **14**, 244–247.
25 P. Mohanty, T. Kang, B. Kim and J. Park, *J. Phys. Chem. B*, 2006, **110**, 791–795.
26 A. Qin, Y. Fang, P. Tao, J. Zhang and C. Su, *Inorg. Chem.*, 2007, **46**, 7403–7409.
27 A. K. Samal and T. Pradeep, *J. Phys. Chem. C*, 2010, **114**, 5871–5878.
28 A. K. Samal and T. Pradeep, *J. Phys. Chem. C*, 2009, **113**, 13539–13544.
29 H.-W. Liang, S. Liu, Q.-S. Wu and S.-H. Yu, *Inorg. Chem.*, 2009, **48**, 4927–4933.
30 G. Zhang, Q. Yu, Z. Yao and X. Li, *Chem. Commun.*, 2009, 2317–2319.
31 G. Zhang, B. Kirk, L. A. Jauregui, H. Yang, X. Xu, Y. P. Chen and Y. Wu, *Nano Lett.*, 2012, **12**, 56–60.
32 H. Fan, Y. Zhang, M. Zhang, X. Wang and Y. Qian, *Cryst. Growth Des.*, 2008, **8**, 2838–2841.
33 G. D. Moon, S. Ko, Y. Xia and U. Jeong, *ACS Nano*, 2010, **4**, 2307–2319.
34 J. Hu, Y. Bando and D. Golberg, *J. Mater. Chem.*, 2009, **19**, 330–343.
35 W. Wang, X. Lu, T. Zhang, G. Zhang, W. Jiang and X. Li, *J. Am. Chem. Soc.*, 2007, **129**, 6702–6703.
36 W. Wang, G. Zhang and X. Li, *Chem. Lett.*, 2008, **37**, 848–849.
37 W. Wang, J. Goebl, L. He, S. Aloni, Y. Hu, L. Zhen and Y. Yin, *J. Am. Chem. Soc.*, 2010, **132**, 17316–17324.
38 A. K. Samal and T. Pradeep, *Nanoscale*, 2011, **3**, 4840–4847.
39 R. D. Robinson, B. Sadtler, D. O. Demchenko, C. K. Erdonmez, L.-W. Wang and A. P. Alivisatos, *Science*, 2007, **317**, 355–358.
40 M. Kobayashi, K. Ishikawa, F. Tachibana and H. Okazaki, *Phys. Rev. B*, 1988, **38**, 3050.
41 R. Xu, A. Husmann, T. F. Rosenbaum, M. L. Saboungi, J. E. Enderby and P. B. Littlewood, *Nature*, 1997, **390**, 57–60.
42 I. Chuprakov, *Appl. Phys. Lett.*, 1998, **72**, 2165.
43 Y. Sun, *Appl. Phys. Lett.*, 2003, **82**, 1440.
44 M. Fujikane, K. Kurosaki, H. Muta and S. Yamanaka, *J. Alloys Compd.*, 2005, **393**, 299–301.
45 F. Li, C. Hu, Y. Xiong, B. Wan, W. Yan and M. Zhang, *J. Phys. Chem. C*, 2008, **112**, 16130–16133.
46 M. Kirsanova, A. Nemchinov, N. N. Hewa-Kasakarage, N. Schmall and M. Zamkov, *Chem. Mater.*, 2009, **21**, 4305–4309.
47 D. Seo, C. I. Yoo, J. Jung and H. Song, *J. Am. Chem. Soc.*, 2008, **130**, 2940–2941.
48 K. Park and R. A. Vaia, *Adv. Mater.*, 2008, **20**, 3882–3886.
49 X. Guo, Q. Zhang, Y. Sun, Q. Zhao and J. Yang, *ACS Nano*, 2012, **6**, 1165–1175.
50 I. Karakaya and W. T. Thompson, *J. Phase Equilib.*, 1991, **12**, 56–63.
51 W. L. Magnus, B. W. Jakob, W. Mathias, H. Paul, E. F. Linus, S. Lars and L. R. Wallenberg, *Nanotechnology*, 2007, **18**, 015504.
52 H. Cölfen and S. Mann, *Angew. Chem., Int. Ed.*, 2003, **42**, 2350–2365.
53 Z.-H. Lin, Y.-W. Lin, K.-H. Lee and H.-T. Chang, *J. Mater. Chem.*, 2008, **18**, 2569–2572.
54 F. Xiao, G. Chen, Q. Wang, L. Wang, J. Pei and N. Zhou, *J. Solid State Chem.*, 2010, **183**, 2382–2388.